Earthquake Engineering & Structural Dynamics
The Journal of the International Association for Earthquake Engineering

EARTHQUAKE ENGINEERING & STRUCTURAL DYNAMICS
Earthquake Engng Struct. Dyn. 2014; **43**:225–246
Published online 9 July 2013 in Wiley Online Library (wileyonlinelibrary.com). DOI: 10.1002/eqe.2340

Site response analysis with two-dimensional numerical discontinuous deformation analysis method

Huirong Bao, Gony Yagoda-Biran and Yossef H. Hatzor*,†

Department of Geological and Environmental Sciences, Ben-Gurion University of the Negev, Beer-Sheva 84105, Israel

SUMMARY

The capability of the numerical discontinuous deformation analysis (DDA) method to perform site response analysis is tested. We begin with modeling one-dimensional shear wave propagation through a stack of horizontal layers and compare the obtained resonance frequency and amplification with results obtained with SHAKE. We use the algorithmic damping in DDA to condition the damping ratio in DDA by changing the time step size and use the same damping ratio in SHAKE to enable meaningful comparisons. We obtain a good agreement between DDA and SHAKE, even though DDA is used with first order approximation and with simply deformable blocks, proving that the original DDA formulation is suitable for modeling one-dimensional wave propagation problems. The ability of DDA to simulate wave propagation through structures is tested by comparing the resonance frequency obtained for a multidrum column when modeling it with DDA and testing it in the field using geophysical site response survey. When the numerical control parameters are properly selected, we obtain a reasonable agreement between DDA and the site response experiment in the field. We find that the choice of the contact spring stiffness, or the numerical penalty parameter, is directly related to the obtained resonance frequency in DDA. The best agreement with the field experiment is obtained with a relatively soft contact spring stiffness of $k=(1/25)(E\times L)$ where E and L are the Young's modulus and mean diameter of the drums in the tested column. Copyright © 2013 John Wiley & Sons, Ltd.

Received 5 February 2012; Revised 30 May 2013; Accepted 5 June 2013

KEY WORDS: site response; discontinuous deformation analysis; numerical modeling; wave amplification; algorithmic damping; earthquake engineering

1. INTRODUCTION

The analysis of seismic site response is very important because the amplification of seismic waves in some specific areas can be very strong. Reflections and scattering of seismic waves near the surface, at layers interfaces, or around topographic irregularities often strengthen the consequences of earthquakes. The maximum amplification and corresponding resonance frequency depend on several factors including the thickness of the overlying layers, their shear modulus, damping ratio, and density. Although alternating layer stiffness in the soil column and geometrical basin effects have been cited as the most common sources of amplification, topographic effect has been reported to be a significant source of motion amplification as well. Whereas it is well established that soft soil deposits may amplify ground motion, it is often assumed that hard-rock sites are safe. However, recent studies suggest that rock sites may also exhibit significant amplification, possibly because of their shear wave velocity.

*Correspondence to: Yossef H. Hatzor, Department of Geological and Environmental Sciences, Ben-Gurion University of the Negev, Beer-Sheva 84105, Israel.
†E-mail: hatzor@bgu.ac.il

Copyright © 2013 John Wiley & Sons, Ltd.

Ground motions developed near the surface are typically attributed to upward propagation of shear waves from an underlying rock formation. If the ground surface, the rock surface or the boundaries between different soil layers are inclined, analyses of the response of the soil deposit can only be made by numerical techniques. If however the ground surface, the rock surface and the boundaries between soil layers are essentially horizontal, the lateral extent of the deposit has no influence on the response and the deposit may be considered as a series of semi-infinite layers. In such cases the ground motions induced by a seismic excitation at the base are the result of only shear deformations in the soil and the deposit may be considered as a one-dimensional shear beam. Site response in this case may be estimated using well developed, one-dimensional computational approaches, such as the program SHAKE [15, 22].

In this paper, we explore the possibility of performing two-dimensional site response analysis in a discontinuous medium. We employ for this purpose the dynamic, implicit, discrete-element numerical discontinuous deformation analysis (DDA) method [23]. We first verify wave propagation modeling capabilities of DDA by comparing one-dimensional site response analysis results with those obtained with SHAKE for the same horizontally layered medium. We then proceed with two-dimensional site response analysis by comparing DDA results with an experimental site response survey performed in the field for a tall and slender limestone multidrum column situated in a historic monument dated back to the Hellenistic period.

As an implicit numerical method, DDA is similar in essence to the FEM. Both methods employ displacement type unknowns and obtain governing equations from the total potential energy of the system. Nevertheless, the difference between FEM and DDA is also significant. Whereas the displacements of nodes are the unknowns in the FEM, in the DDA method, the unknowns are the displacements and deformations of blocks. The displacement compatibility is automatically satisfied by the displacement function in the FEM, whereas it is achieved by the contact conditions between blocks in the DDA method. When the blocks are in contact in DDA, Coulomb's law is applied to the contact interface, and the simultaneous equilibrium equations are formulated and solved repeatedly for each time step. The simultaneous equilibrium equations are obtained from minimization of the total potential energy of the block system.

Discontinuous deformation analysis uses a penalty method to treat contacts. The penalties, in the form of stiff springs, are applied at contact interfaces to prevent either penetration or tension between blocks. It will be shown here that in dynamic DDA applications, the choice of the penalty parameter is crucial for obtaining accurate results. To alleviate the strong dependency of the results on the choice of the penalty parameter, alternative contact algorithms using for example the Lagrange multiplier or augmented Lagrange methods have been proposed [13, 3, 21]. The purpose of this paper, however, is not to enhance the original DDA contact algorithm but to test its applicability to dynamic analysis of block systems by performing sensitivity analyses using analytical solutions and field test data. We believe that testing the applicability of alternative contact algorithms would require similar calibration studies, which are beyond the scope of this paper.

A comprehensive review of the essentials of DDA is provided by [9]. Results of a decade of DDA validation and verification studies from all over the world are reviewed by [16]

1.1. Theoretical background

In the DDA method, the simultaneous equilibrium equations can be written as follows:

$$\mathbf{M}\ddot{\mathbf{d}} + \mathbf{C}\dot{\mathbf{d}} + \mathbf{K}\mathbf{d} = \mathbf{f} \tag{1}$$

that can be derived from minimizing the total potential energy of the system, Π. In Equation (1), **M**, **C**, and **K** are mass matrix, damping matrix, and stiffness matrix, respectively, and **d** and **f** are the displacement unknowns and force vectors. In a two-dimensional DDA model with n blocks, the basic element is a block with six unknowns:

$$\mathbf{d}_i = \left\{ u_0 \quad v_0 \quad r_0 \quad \epsilon_x \quad \epsilon_y \quad \gamma_{xy} \right\}_i^T, \quad (i = 1, 2, \cdots, n) \tag{2}$$

Copyright © 2013 John Wiley & Sons, Ltd.

DOI: 10.1002/eqe

where (u_0,v_0) are the rigid body translations, r_0 is the rotation angle of the block with respect to the rotation center at (x_0,y_0), and ϵ_x, ϵ_y, and γ_{xy} are the normal and shear strains of the block. As shown by Shi [23], the complete first order approximation of displacements at any point (x,y) take the following form:

$$\begin{Bmatrix} u_x \\ u_y \end{Bmatrix}_i = \mathbf{T}_i \mathbf{d}_i \ , \quad (i = 1, 2, \cdots, n) \tag{3}$$

where

$$\mathbf{T}_i = \begin{bmatrix} 1 & 0 & -(y-y_0) & (x-x_0) & 0 & \dfrac{(y-y_0)}{2} \\ 0 & 1 & (x-x_0) & 0 & (y-y_0) & \dfrac{(x-x_0)}{2} \end{bmatrix}_i \tag{4}$$

By adopting first order displacement approximation, the distribution of the stresses and strains are constant in a block, a simplification that limits the accuracy of the DDA method when dealing with wave propagation problems.

Assuming the velocity at the beginning of the time step, which can be obtained from the previous time step, is $\dot{\mathbf{d}}_\mathbf{0}$, and that the time interval of a single time step is Δt, then

$$\begin{aligned} \ddot{\mathbf{d}} &= \frac{2}{\Delta t^2}\left(\mathbf{d} - \Delta t \dot{\mathbf{d}}_\mathbf{0}\right) \\ \dot{\mathbf{d}} &= \frac{2}{\Delta t}\mathbf{d} - \dot{\mathbf{d}}_\mathbf{0} \end{aligned} \tag{5}$$

By substituting Equation (5) into Equation (1), the simultaneous equilibrium equations can be rewritten as

$$\hat{\mathbf{K}} d = \hat{\mathbf{f}} \tag{6}$$

where $\hat{\mathbf{K}}$ is the equivalent global stiffness matrix. Equation (6) can be written in a submatrix form as follows:

$$\begin{bmatrix} \hat{\mathbf{K}}_{11} & \hat{\mathbf{K}}_{12} & \hat{\mathbf{K}}_{13} & \cdots & \hat{\mathbf{K}}_{1n} \\ \hat{\mathbf{K}}_{21} & \hat{\mathbf{K}}_{22} & \hat{\mathbf{K}}_{23} & \cdots & \hat{\mathbf{K}}_{2n} \\ \hat{\mathbf{K}}_{31} & \hat{\mathbf{K}}_{32} & \hat{\mathbf{K}}_{33} & \cdots & \hat{\mathbf{K}}_{3n} \\ \vdots & \vdots & \vdots & \ddots & \vdots \\ \hat{\mathbf{K}}_{n1} & \hat{\mathbf{K}}_{n2} & \hat{\mathbf{K}}_{n3} & \cdots & \hat{\mathbf{K}}_{nn} \end{bmatrix} \begin{Bmatrix} \mathbf{d}_1 \\ \mathbf{d}_2 \\ \mathbf{d}_3 \\ \vdots \\ \mathbf{d}_n \end{Bmatrix} = \begin{Bmatrix} \hat{\mathbf{f}}_1 \\ \hat{\mathbf{f}}_2 \\ \hat{\mathbf{f}}_3 \\ \vdots \\ \hat{\mathbf{f}}_n \end{Bmatrix} \tag{7}$$

where $\hat{\mathbf{K}}_{ij}(i,j = 1, 2, \cdots, n)$ are 6×6 submatrices, $\mathbf{d}_i$ and $\hat{\mathbf{f}}_i(i = 1, 2, \cdots, n)$ are 6×1 submatrices corresponding to block i.

2. SITE RESPONSE ANALYSIS: DISCONTINUOUS DEFORMATION ANALYSIS VERSUS SHAKE

The SHAKE program uses a lumped-mass type of approach to analyze the response of a soil deposit consisting of irregularly varying, but linearly elastic, soil properties. The soft deposit, which may consist of several layers of varying properties, is idealized by a series of lumped masses

Copyright © 2013 John Wiley & Sons, Ltd.

DOI: 10.1002/eqe

interconnected by springs that resist lateral deformations. These springs represent the stiffness properties of the material between any two lumped masses. Damping is assumed to be linearly viscous in SHAKE. When the layer is subjected to a horizontal seismic motion through its base, the equation of motion of the system may be represented in a matrix form as follows:

$$\mathbf{M}\ddot{\mathbf{u}} + \mathbf{C}\ \dot{\mathbf{u}} + \mathbf{K}\mathbf{u} = \mathbf{g}(t) \tag{8}$$

where **M**, **C**, and **K** are the mass, viscous damping, and stiffness matrices, respectively; $\mathbf{g}(t)$ is the earthquake load vector, and **u** is the relative displacement vector. These matrices and vectors are of order N, where N is the number of lumped masses used in idealizing the layer in a program such as SHAKE.

The basic mechanism of amplification is best illustrated by examining the effect of an un-damped elastic surface layer on incoming bedrock motions.

For a uniform layer of isotropic, linear elastic, soil overlying a rigid bedrock unit as shown in Figure 1, the amplification function for an un-damped soil layer is [12]

$$|F_1(\omega)| = \frac{1}{|\cos(\omega H/v_s)|} \tag{9}$$

and for a damped soil layer is

$$|F_2(\omega)| = \frac{1}{\sqrt{\cos^2(\omega H/v_s) + \left(\xi\omega H/v_s\right)^2}} \tag{10}$$

where H is the thickness of the soil layer, v_s is the shear wave velocity, ξ is the damping ratio of the soil layer, and ω is the angular frequency of the ground motion.

2.1. Finding an equivalent damping ratio in dynamic discontinuous deformation analysis simulations

One might think that it should be possible to determine the damping matrix for the modeled structure from the damping properties of individual structural elements, just as the structural stiffness matrix is determined. However, it is impractical to determine the damping matrix in this manner because there is no obvious connection between the damping properties and the structural dimensions, structural member sizes, and the structural materials [4]. Even if the damping properties of each structural element were known, the resulting damping matrix would not account for a significant part of the energy dissipated in friction at joint interfaces. The energy dissipation mechanism in a joint is a complex process, which is largely influenced by the interface pressure and the joint properties. Normally, a Rayleigh damping matrix, also known as classical damping matrix, is a standard choice in numerical simulations. However, if the system consists of two or more components with significantly different damping properties, a non-classical damping matrix must be used.

To simulate a real dynamic problem with DDA, damping should be considered. In the original DDA code, a damping submatrix was not incorporated in the equilibrium equations. To account for additional energy dissipation mechanisms, a so called 'kinetic damping factor' is provided in the original code. The user specified 'kinetic damping' factor arbitrarily forces the velocities at the next time step to be reduced by some percentage of that in the current step, to account for other energy

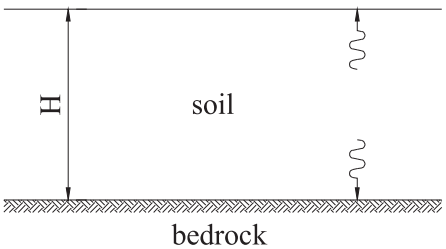

Figure 1. Linear elastic soil deposit of thickness H underlain by rigid bedrock.

Copyright © 2013 John Wiley & Sons, Ltd.

DOI: 10.1002/eqe

loss mechanisms that may take place during dynamic deformation in the block system, such as fracturing and crushing at block tips, and shear heating during high velocity sliding. However, an arbitrary application of 'kinetic damping' can completely distort the structural vibrations, even if only 1% kinetic damping is applied. Consider for example, a cantilever beam clamped on one side, 10-m long and 1-m high, composed by 10 1 $\times$ 1 m blocks (Figure 2). A triangular impulse (Figure 3) is applied at the free end of the beam as an initial disturbance. The resulting vertical displacement time history of the free end of the beam is plotted in Figure 4. Theoretically, the cantilever beam should start free vibrations after 0.02 s, as obtained with the 'full dynamic' solution; yet, the motion is totally damped when even 1% kinetic damping is applied, as shown by the dashed curve.

Indeed, the best way to model structural damping in DDA would be to incorporate a damping submatrix in the simultaneous equations of equilibrium (Equation (1)). Proper implementation of a structural damping submatrix in DDA is complex because it requires consideration of the contact scheme, joint material, and block material. Furthermore, it requires determination of the viscosity

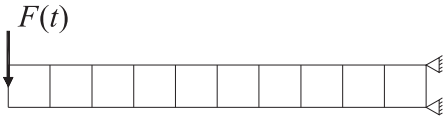

Figure 2. Configuration of the discontinuous deformation analysis cantilever beam model. $F(t)$ is the dynamic load applied at the free end.

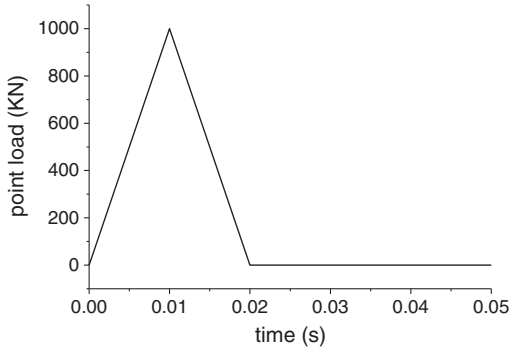

Figure 3. Time history of the input point load.

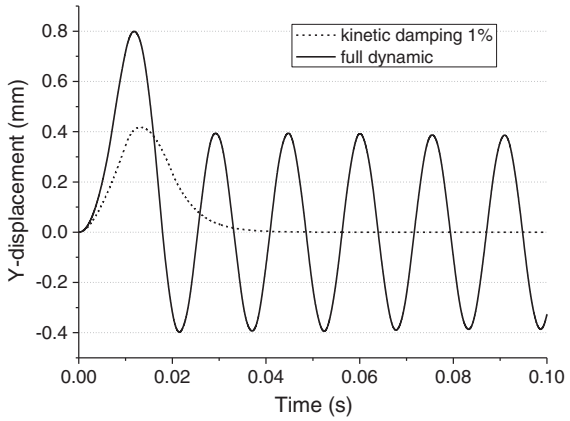

Figure 4. y-direction displacement of the free end of the cantilever beam obtained with discontinuous deformation analysis for un-damped (solid line) and 1% kinetic damping (dashed).

Copyright © 2013 John Wiley & Sons, Ltd.

DOI: 10.1002/eqe

coefficient of the elements in the block system, which in most cases is largely unknown. A comprehensive treatment of these issues, which requires further research, is beyond the scope of this paper. Instead, we present an alternative damping scheme that is equivalent to the 'damping ratio' that is used in SHAKE and similar programs, thus allowing proper comparisons between DDA and SHAKE outputs.

In many numerical methods, inherent 'numerical damping', also referred to as 'algorithmic damping' [6], does exist. The numerical damping is typically associated with the time integration scheme used for integrating second order systems of equations over time. Numerical damping stabilizes the numerical integration scheme by damping out the unwanted high frequency modes. For the Newmark scheme, numerical damping also affects the lower modes and reduces the accuracy of integration scheme from second order to first order. Higher modes are more susceptible to error propagation than lower modes. Therefore, numerical damping is desirable for suppressing higher mode errors. In DDA, the numerical damping that is associated with the time integration scheme increases with increasing time step size. If the time step is small enough, the numerical damping phenomenon is insignificant. However, a time step size that is too small may cause difficulties in the convergence of the numerical solution. To obtain an equivalent damping ratio for DDA, we utilize the algorithmic damping without any further modifications, by seeking the time step size that will result in exactly the same damping ratio that would have been assumed otherwise in the structural analysis.

Our suggested scheme for obtaining an equivalent damping ratio from the algorithmic damping in DDA is further illustrated by the cantilever beam model shown in Figure 2. Two time step sizes are applied to the beam when loaded with the same time history (Figure 3). The beam starts free vibration after 0.02 s when the exciting force is removed. The y-direction displacement time history of the free end is shown in Figure 5. A very significant attenuation of the amplitude is observed when the time step size is increased by one order of magnitude from $1e^{-5}$ to $1e^{-4}$ s, confirming our suggestion that the magnitude of algorithmic damping in DDA depends upon the size of the time step used.

Generally, the damping ratio of an oscillating system in one direction (ζ) can be obtained from the attenuation of the steady free vibration using the following expression:

$$\zeta = \frac{1}{2\pi n} \ln \frac{A_0}{A_n} \tag{11}$$

where A_0 and A_n are amplitudes of the first and the n-th wave crests, respectively, and n is the number of cycles. Utilizing Equation (11), we can now find the equivalent damping ratio obtained using the algorithmic damping in DDA as a function of time step size.

When trying to find the equivalent damping ratio from DDA output, it is necessary to investigate another numerical control parameter and its possible influence on the results—the stiffness of the

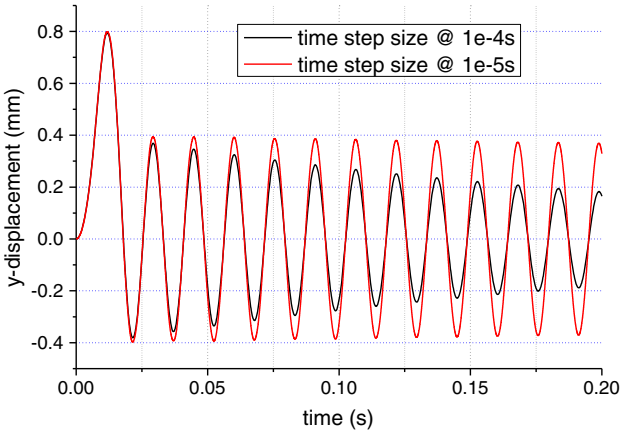

Figure 5. Damping in y-direction as measured at the free end of the cantilever beam (Figure 2) utilizing the algorithmic damping in discontinuous deformation analysis.

Copyright © 2013 John Wiley & Sons, Ltd.

DOI: 10.1002/eqe

contact spring used as penalty in DDA. Our numerical tests clearly show that the choice of the penalty value has no obvious effect on the equivalent damping ratio that is obtained. We fixed the time step size to $1e^{-5}$ s and varied the penalty value by three orders of magnitude, from 1E to 100E (where E is Young's modulus). With increasing penalty value, the natural frequency of the beam also increased, whereas the maximum displacement decreased, as shown in Figure 6. The same result would have been obtained had we changed the elastic modulus of the blocks comprising the beam, as in either way, the effective stiffness of the beam is changed.

2.2. Finding the optimal numerical control parameters for dynamic discontinuous deformation analysis simulations

In dynamic analysis, both temporal and spatial resolution of a numerical model are critical to ensure convergence of the results. Similar to the FEM, the accuracy of the DDA method depends on the ratio (η) obtained by dividing the length of the side of the largest element in the modeled domain by the minimum wavelength of elastic waves propagating through the system:

$$\eta = \frac{\Delta x}{\lambda} \tag{12}$$

where λ is the wavelength, and Δx is the side length of the element along the direction of wave propagation path. Typically in FEM models, the optimal ratio η should be smaller than approximately 1/12 for obtaining most accurate results [14]. Furthermore, in modeling nonlinear propagation of sound waves, Kagawa *et al*. [10] recommended element size smaller than one-twentieth of the primary wavelength. Considering computational efficiency, Moser *et al*.[19] recommended the optimized size of elements to be one-twentieth of the shortest wavelength. To avoid spurious reflections of elastic waves between elements due to the change of element sizes, the largest element size is recommended to be smaller than one-tenth of the wavelength [2].

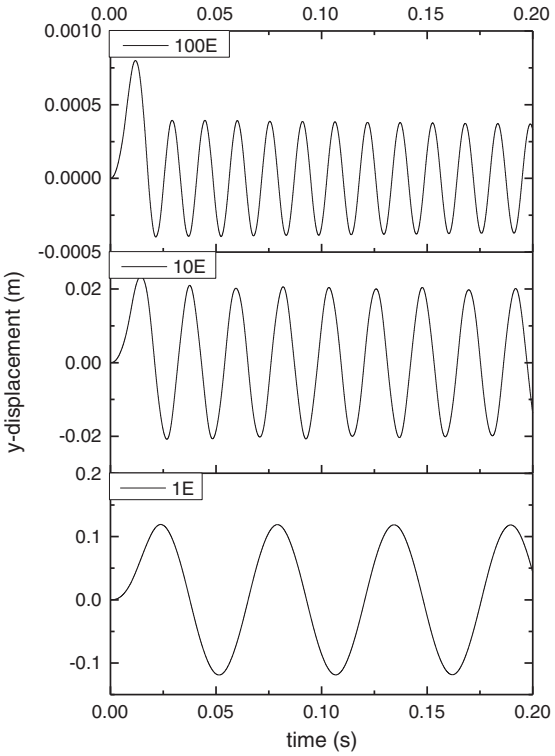

Figure 6. Relationship between penalty value and numerical damping in discontinuous deformation analysis. Time step size in all simulation equals $1e^{-5}$ s.

Copyright © 2013 John Wiley & Sons, Ltd.

DOI: 10.1002/eqe

Choosing a proper time step size is also very important for the stability and accuracy of the solution in DDA [6]. In general, the accuracy of the model can be increased with the decrease of time step intervals. With time step intervals that are too long, the high frequency components are not resolved accurately enough. However, too small time steps may induce pseudo high frequency oscillations at the wave front. Too small time steps also require significantly more computation time. A compromise is therefore necessary between these conflicting considerations. In FEM simulation of nonlinear sound wave propagation, Kagawa *et al*. [10] recommended the time step should be chosen smaller than one-hundredth of the primary wave period. For Newmark time integration scheme, the optimized time step size is one-twentieth of the smallest period of incident waves, which gives accurate solutions in an efficient manner [19]. To avoid bifurcation in the DDA solution, the time step size should satisfy the following requirement [6]:

$$\Delta t < \frac{4}{\omega_{\max}} \tag{13}$$

where $\omega_{\max}$ is the maximum un-damped frequency of vibration of the system described by Equation (1). Equation (13) is a necessary condition for the stability of the solution. Because normally the natural frequency of the system is not known in advance in DDA and is difficult to obtain from the system of equilibrium equations (Equation (1)), application of this criterion is not always possible.

According to the Courant–Friedrichs–Levy condition [5] to ensure stability of numerical methods when solving one-dimensional wave propagation problems, the time step size should satisfy

$$\Delta t < \frac{\Delta x}{v} \tag{14}$$

where v is the wave velocity, and Δx has the same meaning as that in Equation (12). The CFL condition is only a necessary condition for convergence when solving partial differential equations.

From Equation (12) earlier, we have $\Delta x = \eta\lambda$; substituting into Equation (14) with $\lambda = vT$, we obtain

$$\Delta t < \frac{\eta\lambda}{v} = \eta T \tag{15}$$

where T is the period of incident wave. Note that Equation (15) does not ensure accuracy, but guarantees convergence of the numerical solution. Finally, in simulating P-wave propagation with DDA,Gu and Zhao [8] recommended the block size to be one-sixteenth of the wavelength, for one-dimensional P-wave propagation problems, considering both computation accuracy and efficiency. There is no reference to S-wave propagation in their work, however. It is important to point out here that in DDA even when the time step size does satisfy the requirement of Equation (15) algorithmic damping may still be significant (Figure 5).

To study the effect of time step size and block size on the solution accuracy in DDA when modeling one-directional shear wave propagation through a layered medium, consider the DDA model shown in Figure 7. The shear wave is generated in the model by inducing horizontal movements at the base, which is supported on four pin points, typically referred to as 'fixed points' in DDA. The four pin points are loaded simultaneously by a horizontal motion with time history as shown in Figure 8.

A series of numerical tests with different η values is carried out. We find that the relative error with respect to wave amplitude at measurement point M1 decreases with decreasing η as shown in Figure 9.

The relative error with respect to amplitude is defined here by

$$e = \frac{|A_0 - A_m|}{A_0} \times 100\% \tag{16}$$

where A_0 is the analytical amplitude of the incident wave at the measurement points; A_m is the numerically obtained amplitude at the same measurement point with DDA. Because the DDA blocks are linear elastic and un-damped, the analytical amplitude in the tests is the same amplitude as that of the incident wave at the rigid base. The relative errors with respect to amplitude plotted in

Copyright © 2013 John Wiley & Sons, Ltd.

DOI: 10.1002/eqe

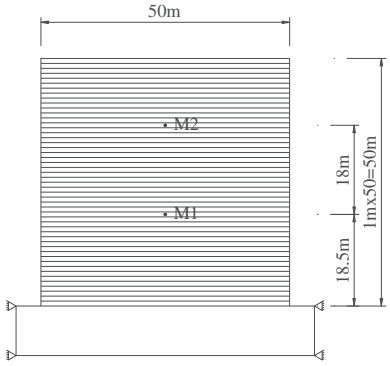

Figure 7. Configuration of the one-dimensional shear wave propagation discontinuous deformation analysis model.

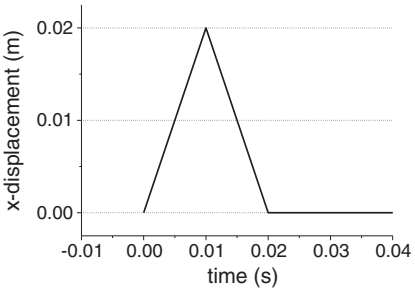

Figure 8. Triangular incident wave time history used in discontinuous deformation analysis model for one-dimensional shear wave propagation (Figure 7).

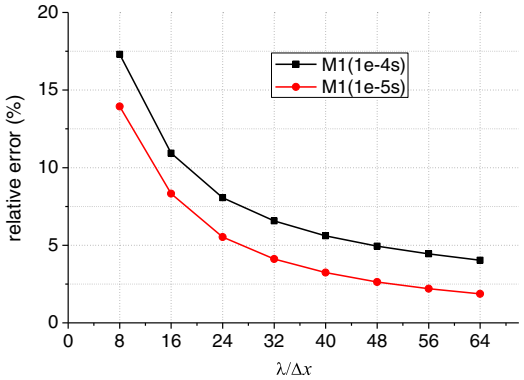

Figure 9. Relationship between relative error and the ratio of wavelength over element size, where $\lambda/\Delta x = \eta^{-1}$.

Figure 9 includes the numeric error caused by algorithmic damping. Because larger time step size results in increased algorithmic damping, the obtained relative errors with time step size of $1e^{-4}$ s are larger than with time step size of $1e^{-5}$ s, and the differences between them remains largely the same for every ratio η. Moreover, inspection of Figure 9 also reveals that for both time step sizes the rate of change of the relative error decreases with decreasing η. Therefore, we conclude that the effect of the ratio η on the solution error is independent of the time step size.

The analysis of the numerical error thus far considered the amplitude only, and as can be inferred from Figure 9 clearly, the numeric error decreases with decreasing ratio η. This is not true, however,

Copyright © 2013 John Wiley & Sons, Ltd.

DOI: 10.1002/eqe

when the wave velocity is used to obtain the numeric error using a similar expression as Equation (16) and replacing amplitude with velocity. Recall that in DDA, a penalty method is employed to treat contacts between blocks so that the displacement compatibility is satisfied. Yet, penalty methods can only reach an approximate satisfaction of the displacement compatibility, which depends on the choice of the penalty value (i.e., the stiffness of the contact spring). An increasing number of artificial joints along the wave propagation path will therefore inevitably slow down the numerical wave propagation velocity, especially when a low penalty value is employed. An optimal penalty value that is typically recommended for DDA applications is 40 times the value of the Young's modulus of the blocks. Our experience with modeling one-dimensional shear wave propagation problems (results not reported here for brevity) indicates that a penalty value higher than 100 times the Young's modulus of blocks would allow better accuracy of wave propagation velocity.

To minimize the effect of the number of contacts on the solution, we keep the number of interfaces per unit length along the wave propagation path constant in our simulations. We therefore vary the ratio η in each simulation by changing the wavelength λ of the incident wave. The wavelength of a shear wave can be obtained by

$$\lambda = T\sqrt{\frac{G}{\rho}} \tag{17}$$

where T is the period of the incident wave, G is the shear modulus of blocks, and ρ is the unit mass. Although in principal the wavelength could be varied by changing any one of the three parameters in Equation (17), changing T may induce errors due to the different frequencies. It would be better, therefore, to change either the shear modulus or the unit mass to obtain different wavelengths in each numerical test.

In addition to the amplitude error, it is necessary to verify the preservation of wave shape during propagation. A one-cycle sinusoidal horizontal displacement function (Figure 10) is used as input for each pin point in the model shown in Figure 7 and four different wavelength ratios, $\eta^{-1} = 4$, 8, 16, and 32, are tested.

The displacement time history of measurement point M1 is shown in Figure 11. It is found that the wave shape is well resolved for both wave crest and wave trough for $\eta^{-1} = 16$ and beyond. We also find that decreasing time step size has no effect on the preservation of the wave shape (data not reported here for brevity) because the preservation of wave shape is a spatial resolution of the wave.

2.3. Verification of one-dimensional site response analysis with discontinuous deformation analysis using SHAKE

To check the possibility to perform accurate site response analysis with DDA, with all the considerations regarding optimal numerical control parameters and an equivalent damping ratio discussed earlier in mind, we begin with a one-dimensional problem that can be computed by means of an alternative, well established, computational method. We chose the program SHAKE for our verification because its algorithm has been verified by many workers and its accuracy is well established for the underlying assumptions and boundary conditions.

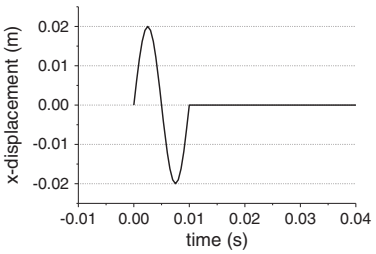

Figure 10. One-cycle sinusoidal incident wave time history used to induce vertical shear wave propagation in the discontinuous deformation analysis model shown in Figure 7.

Copyright © 2013 John Wiley & Sons, Ltd.

DOI: 10.1002/eqe

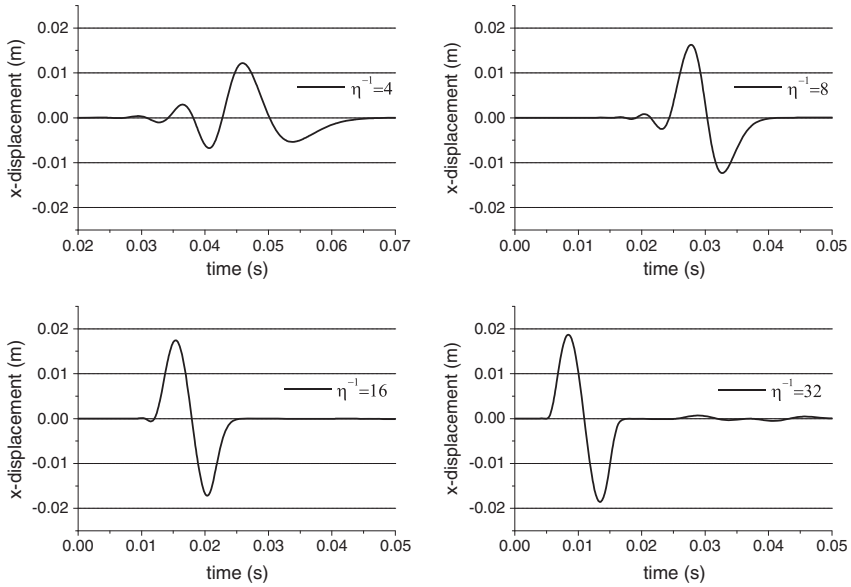

Figure 11. Wave forms as obtained with discontinuous deformation analysis at M1 (for model shown in Figure 7) for different wavelength ratios. The time interval in all four simulations is kept at $\Delta t = 1e^{-4}$ s.

Consider the DDA model shown in Figure 12 with material properties and control parameters as listed in Table I. The two-dimensional model is created with layer length to layer width ratio sufficiently high (15) so as to simulate one-dimensional vertical propagation of shear waves from the excited foundation block through the stack of the horizontal layers, topped by the surface layer. A real earthquake time history (Figure 14) is applied to the four fixed points at the foundation block as in the verification tests earlier, in the horizontal direction only. The shear waves are then allowed to propagate vertically through the stack of 15 horizontal layers, each 15-m long and 1-m thick. The response is measured at the two measurement points M1 and M2 at the foundation block and surface layer, respectively. The same geometrical configuration is modeled with SHAKE (Figure 13), with 15 horizontal layers of infinite lateral extent, each of 1 m thickness. The only difference in the loading scheme is that whereas in the DDA, model the foundation block is excited by time dependent displacements, in SHAKE, the excitation at the bedrock layer is in acceleration. In both methods, the excitation is restricted to the foundation block and the response is measured at the top layer (M2) with respect to the foundation layer (M1). The two records used are shown in Figure 14.

To compare between the two different computational methods, the obtained spectral amplifications are plotted in Figure 15. For the DDA model, the maximum amplification is 29.07 and the resonance frequency is 13.95 Hz; for the SHAKE model, the maximum amplification is 28.93 at frequency

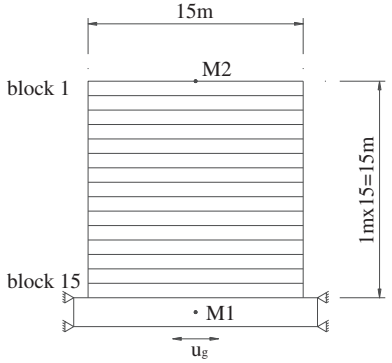

Figure 12. Configuration of the layer structure for the discontinuous deformation analysis model.

Copyright © 2013 John Wiley & Sons, Ltd.

DOI: 10.1002/eqe

Table I. Discontinuous deformation analysis parameters for the 15-layer model.

Joint material	Friction angle	50°
	Cohesion strength (MPa)	100
	Tensile strength (MPa)	50
Control parameter	Dynamic factor	1.0
	Penalty stiffness (GN/m)	1500
	Time step size (s)	1×10^{-3}
	Maximum displacement ratio	0.0008
	Successive over relaxation factor	1.5
	Total time steps	60,000
Block material	Density (kg/m^3)	2643
	Young's modulus (GPa)	4.788
	Poisson ratio	0.25

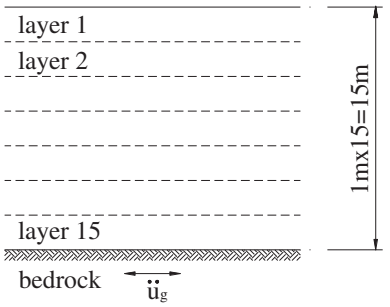

Figure 13. Schematic illustration of the SHAKE model

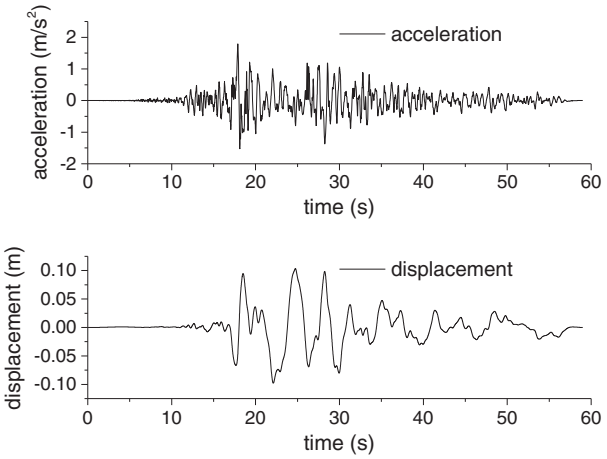

Figure 14. Input ground motion (CHI-CHI 09/20/99, ALS, E (CWB)).

14.21 Hz. The agreement between the two methods for a homogenous layered medium is good, suggesting that accurate site response analysis is possible with DDA, even when higher order terms are neglected (first order approximation) and the blocks are assumed to be simply deformable. Moreover, it is clearly demonstrated here that loading the foundation block with displacement or acceleration time histories is equivalent, an issue that has focused some debate recently [25].

Finally, to verify the capability of DDA to perform one-dimensional site response analysis in an inhomogenous layered medium, consider the DDA model shown in Figure 12 but with mechanical properties for the layers as listed in Table II. The resulting response spectra are shown in Figure 16. The equivalent damping ratio obtained in the DDA model is 2.3%, which is input to the SHAKE model for comparison. Again, the agreement between the two methods is good: the resonance

Copyright © 2013 John Wiley & Sons, Ltd.

DOI: 10.1002/eqe

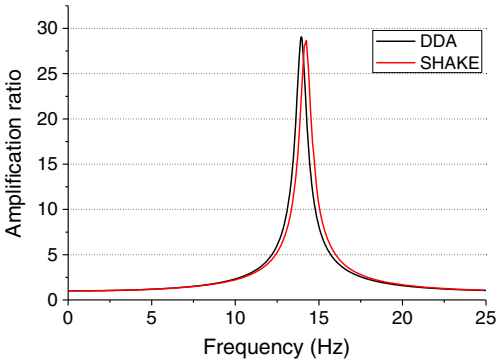

Figure 15. Spectral amplification obtained with discontinuous deformation analysis and SHAKE for 15 horizontal layers of homogenous material properties.

Table II. Material properties of layers/blocks (Figure 16).

Layer/block	Density (kg/m^3)	Young's modulus (GPa)	Shear modulus (GPa)	Poisson ratio
1–3	2403	4.5	1.8	0.25
4–6	2162	4.1	1.64	0.25
7–9	2243	4.2	1.68	0.25
10–12	2483	4.0	1.6	0.25
13–15	2643	4.8	1.92	0.25

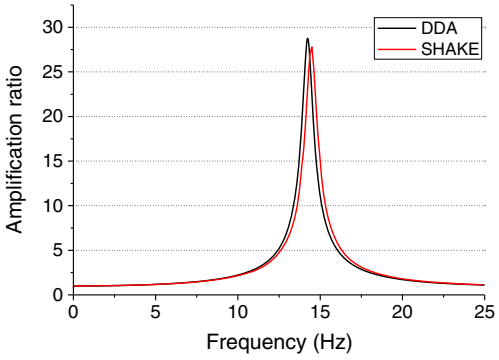

Figure 16. Amplification spectrum for in-homogenous stack of layers with mechanical properties as listed in Table II.

frequency obtained with DDA is 14.23 Hz and with SHAKE 14.50 Hz; the maximum amplification obtained with DDA is 28.76 and with SHAKE is 27.79, namely 3% difference. These results confirm that accurate site response analysis with DDA is possible, provided that the assumed damping ratio is implemented correctly and the numerical control parameters are well conditioned, as explained earlier in this section.

3. DISCONTINUOUS DEFORMATION ANALYSIS VERSUS. GEOPHYSICAL FIELD EXPERIMENT

3.1. Field experiment in the Avdat site

The field experiment was performed in Avdat National Park, a UNESCO world heritage site. Avdat, a major ancient Nabatean road station along the Route of Spices, lies in the central Negev highlands of

Copyright © 2013 John Wiley & Sons, Ltd.

DOI: 10.1002/eqe

southern Israel, 655 m above sea level and 80 m above its surroundings. Avdat was established in the third century BC and was annexed to the Roman Empire at AD 106 along with the entire Nabatean kingdom [20]. Avdat was abandoned at AD 636, never to be occupied again. A strong earthquake that struck the region between AD 631 and 636 is believed to have been the main reason for its abandonment [7]. Indeed, Many buildings in Avdat show evidence of seismic damage, including ones that have been used in the seventh century AD [18].

At the western part of the city, on an elevated terrace, a single multidrum column that was used for supporting the roof of a Nabatean temple stands today following some restoration work (Figure 17).

Site response measurements were performed by the Geophysical Institute of Israel [27]. Four velocity seismometers were placed on the column: two at the top of the column and two nearest to its base. Each pair of seismometers was placed perpendicular to one another in north–south and east–west directions (Figure 18).

The response of the column to three different loading modes was recorded with the velocity seismometers positioned at the top and base of the column as follows: (i) ambient, background, or

Figure 17. The multidrum column at the western terrace of Avdat.

(a) (b) (c)

Figure 18. (a) Velocity seismometers used in field experiment, (b) application of sledgehammer impacts to the base of the column to induce 'dynamic' load, and (c) application of manual push and release to the top of the column to induce 'static' load.

Copyright © 2013 John Wiley & Sons, Ltd.

DOI: 10.1002/eqe

noise; (ii) dynamic load applied at the base of the column by impact of a sledgehammer; and (iii) static load obtained by application of manual push and release at the top of the column (Figure 18). The first and second resonance modes obtained under the three different styles of vibration are similar, with the first resonance mode at 3.0–3.8 Hz and the second mode at 4.2–5.3 Hz (Figure 19).

3.2. Discontinuous deformation analysis validation using field experiment

In this study,,we apply a very small disturbance to multidrum column, either by applying a gentle push at the top or by applying a blow with a sledgehammer at the bottom of the column and compare the

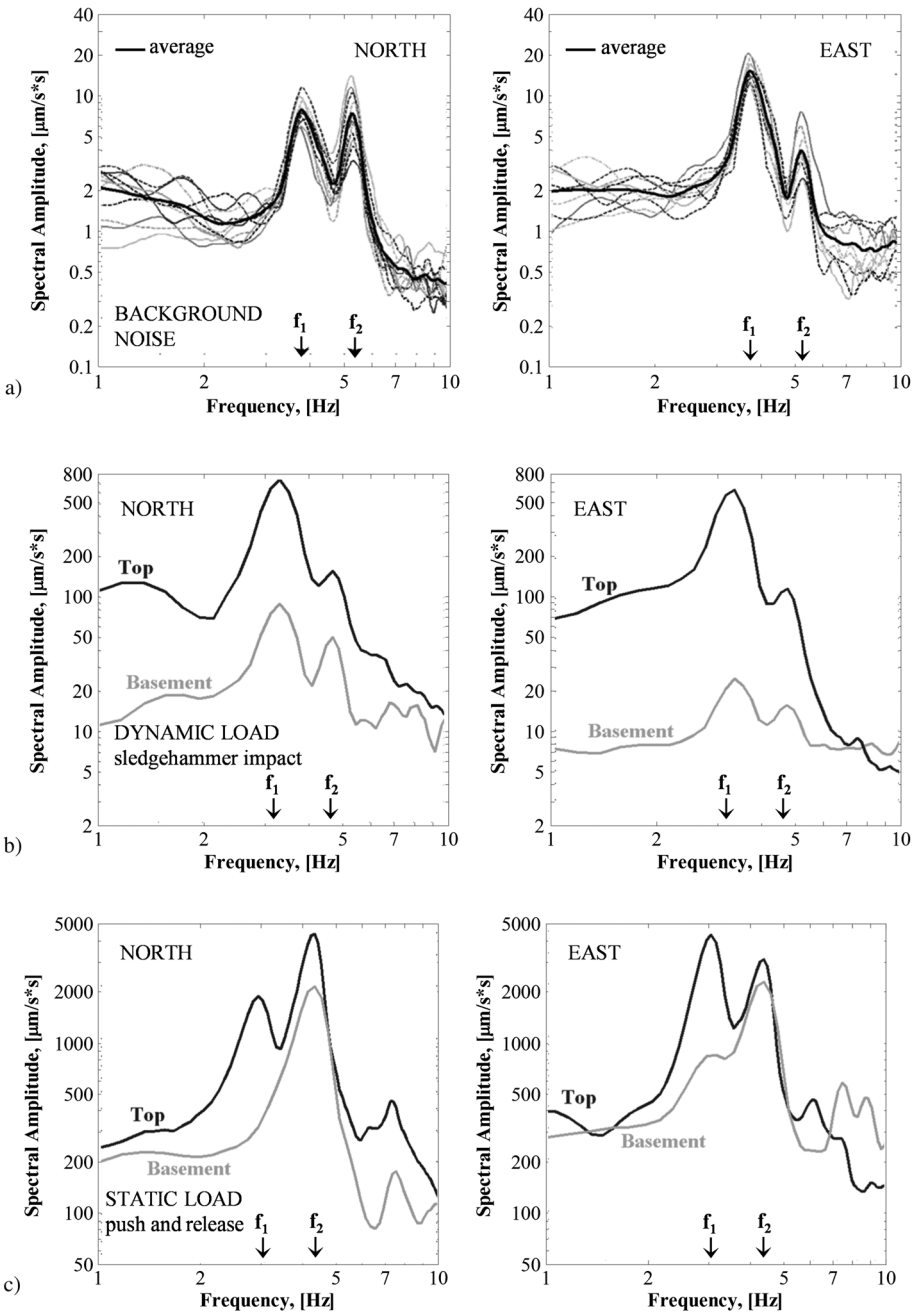

Figure 19. Experimentally obtained Fourier velocity amplitude spectra in North (H332) and East (H748) directions for ambient (a), dynamic (b), and static (c) excitation at the base and top of the column.

Copyright © 2013 John Wiley & Sons, Ltd.

DOI: 10.1002/eqe

response spectra computed with DDA and measured in the field. Because the disturbance is very small, sufficient to induce vibrations but certainly insufficient to trigger rocking (two-dimensional—in plane) or prompt wobbling (three-dimensional—out of plane) motions, we do not expect any out of plane motions between the drums during column vibration. Therefore, a two-dimensional approach is assumed valid in this case, and the calibration of the model is limited to the 'linear' response of the column.

The two-dimensional-DDA mesh is comprised of 11 blocks: one large foundation block, fixed in space by three fixed points and therefore cannot move, and 10 rectangular blocks, placed one on top of the other with proportions similar to the actual column, representing the modeled multidrum column of Avdat. The model is excited in either one of two loading points: one at the lowermost drum, simulating the sledgehammer impacts, or 'dynamic' loading, and one at the uppermost drum, representing the manual push, or 'static' loading (Figure 20).

Before performing simulations under external forces, several models loaded by gravity alone were analyzed to optimize the user defined numerical control parameters, whereas the blocks settle under their own weight. Simulations under gravity only were run for 15 s of real time. Two Δt values were used: 0.01 and 0.001 s. The assumed maximum displacement per time step ratio [23] was set equal to Δt, and sensitivity analysis was performed to optimize the penalty value (k). Two numerical responses to gravitational load were investigated: (i) the time it takes for the initial oscillations of the column in the vertical direction to stabilize, an effect referred to herein as 'gravity turn-on'; and (ii) numerically obtained horizontal displacements of the uppermost block, which naturally have no physical explanation when subjecting the symmetrical column to vertical gravitational loading. The physical and numerical parameters used in the simulations are listed in Table III.

Concentrated results of sensitivity analyses are presented in Table IV. Gravity turn-on is achieved much faster when using the larger time step, because of the algorithmic damping effect discussed earlier. Furthermore, the model experiences smaller horizontal displacements when using larger time step, again, because of the numerical damping effect. The selection of the optimal penalty value for forward modeling was made on the basis of the results of the sensitivity analyses for the smaller time step as it is more sensitive to the change in penalty value. The range of optimal penalty value is between 1×10^8 and 1×10^9 N/m (bold in Table IV).

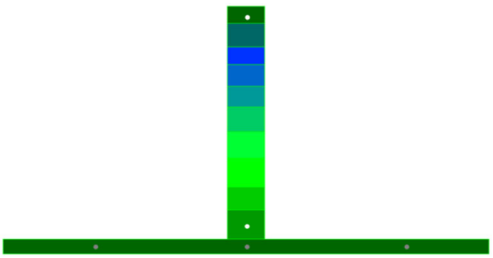

Figure 20. The two-dimensional-discontinuous deformation analysis mesh used in the numerical modeling of the Avdat column. The lowermost block is fixed by three fixed points (grey circles), the mesh is loaded by either of the two loading points (white circles).

Table III. Physical and numerical parameters used in the column simulations.

Parameter	Value
Block density	2250 kg/m^3
Block Young's modulus	17 GPa
Block Poisson's ratio	0.22
Δt (time step size)	0.01–0.001 s
Maximum displacement ratio	Value identical to Δt, dimensionless
k (penalty value)	1×10^7–1×10^{11} N/m

Copyright © 2013 John Wiley & Sons, Ltd.

DOI: 10.1002/eqe

Table IV. Sensitivity analysis of numerical control parameters for gravitational load only using the two-dimensional-discontinuous deformation analysis model shown in Figure 20. All other input parameters are listed in Table III. Legend: Δt = time interval in s, k = penalty value in N/m and **u** = horizontal displacement in cm. Optimal penalty values are in bold.

	$\Delta t = 0.001$		$\Delta t = 0.01$	
k	Real time to gravity turn-on	**u**	Real time to gravity turn-on	**u**
1×10^{7}	Not stable	N/A	Not stable	N/A
5×10^{7}	8	0	1	0.000005
1×10^{8}	**5 to 6**	**0**	1	0.000002
2×10^{8}	**3 to 4**	**0**	0.5	0.000001
3×10^{8}	**2 to 3**	**0**	0.7	0
4×10^{8}	**2 to 3**	**0**	0.7	0
5×10^{8}	**2 to 3**	**0**	N/A	N/A
6×10^{8}	**2 to 3**	**0**	N/A	N/A
7×10^{8}	**2 to 3**	**0**	N/A	N/A
8×10^{8}	**2 to 3**	**0**	0.6	0
9×10^{8}	**2 to 3**	**0**	N/A	N/A
1×10^{9}	**2**	**0**	N/A	N/A
2×10^{9}	2	0	0.55	0
3×10^{9}	2	0.000006	N/A	N/A
4×10^{9}	2	0	N/A	N/A
5×10^{9}	Not stable	Not stable	0.5	0
6×10^{9}	Not stable	Not stable	N/A	N/A
1×10^{10}	Not stable	Not stable	1	0
1×10^{11}	N/A	N/A	1	0
1×10^{13}	N/A	N/A	1	0

As mentioned earlier, load was applied at either of the two loading points marked by white circles in Figure 20. When simulating dynamic impact (sledgehammer blow), force was applied at a single time step of the analysis by a pulse function (Figure 21(a)). When simulating static load (manual push), force was applied as a step function (Figure 21(b)), for a time interval of 1 s.

Dynamic load was applied with values between 10,000 and 300,000 N; column vibrations were not always obtained under the lower load values. Static load was applied with values between 100 and 3000 N; higher load values triggered some initial translation of the uppermost block in the horizontal direction, followed by free vibrations of the column. FFT analysis of a typical result is shown graphically in Figure 22 along with the average curve obtained from the physical experiments.

Note that the results of the field experiment indicate two modes, whereas DDA results indicate only a single mode. This discrepancy could arise from soil structure interactions that may be present in the field but are prohibited in the DDA model because the base block was fixed in the model (Figure 20). For detailed description of the dynamics of multi column drums, see [11, 1].

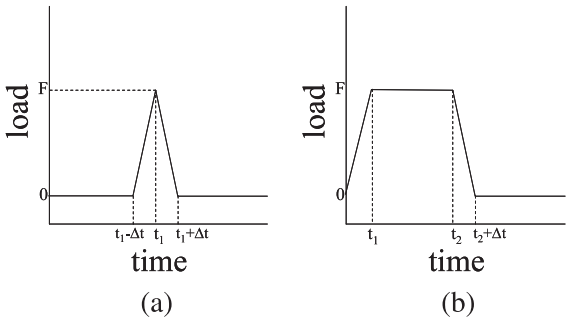

Figure 21. Input loading functions used as input in two-dimensional-discontinuous deformation analysis simulations: (a) dynamic load function used to simulate sledgehammer impulse applied at the base of the column and (b) static load function used to simulate the manual push and release applied manually at the top of the column.

Copyright © 2013 John Wiley & Sons, Ltd.

DOI: 10.1002/eqe

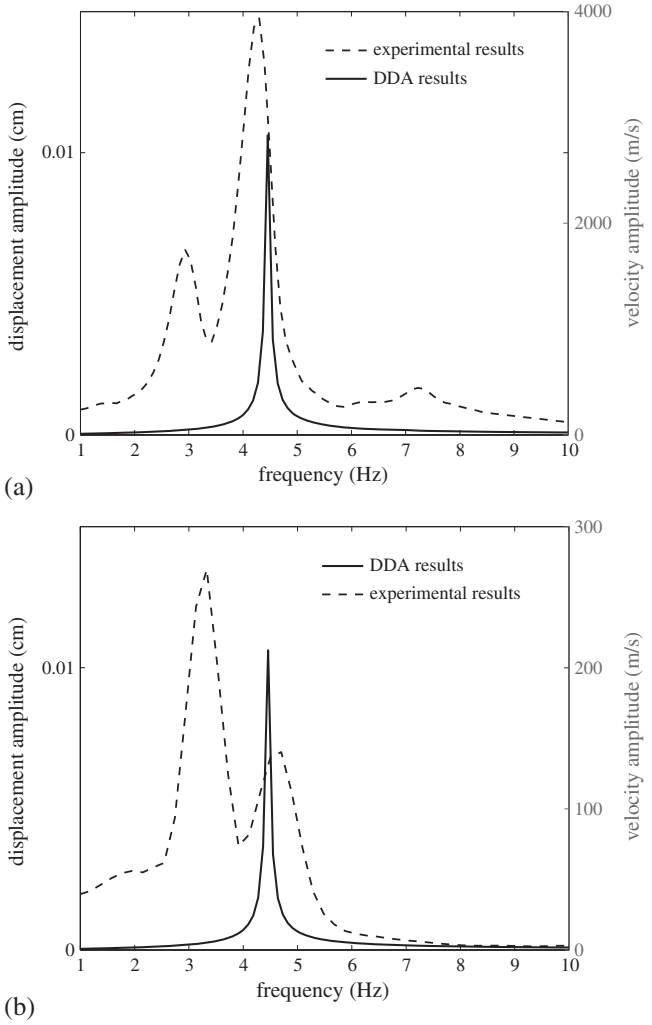

Figure 22. Response spectra of studied column: comparison between discontinuous deformation analysis and experimental results. Discontinuous deformation analysis simulations were executed with penalty value of $4x10^8$ N/m. (a) static loading and (b) dynamic loading.

Concentrated results of dynamic DDA simulations under static and dynamic loading are presented in Table V with the obtaine different values of penalty. Inspection of the results in Table V reveals the following conclusions:

1. The dominant frequency of the modeled system obtained with DDA is highly dependent upon the penalty value. It increases with increasing penalty value from 2.3 Hz with $k = 1\times 10^8$ N/m to 6.3 Hz with $k = 1\times 10^9$ N/m.

Table V. Results of the column response to external 'dynamic' and 'static' forces. The choice of penalty value which returns results that best agree with field experiment is in bold.

Penalty value (N/m)	Dominant frequency (Hz) for dynamic loading	Dominant frequency (Hz) for static loading
1×10^8	2.3–2.4	2.4
2×10^8	3.3	3.3
4×10^8	**4.2–4.3**	**4.3–4.5**
7×10^8	5.1	5.1–5.2
1×10^9	5.9–6	5.9, 6.2–6.3

Copyright © 2013 John Wiley & Sons, Ltd.

DOI: 10.1002/eqe

2. The dominant frequency of the modeled system as obtained with DDA does not depend on the loading mechanism or the magnitude of the applied force; similar values are obtained for both static and dynamic loading for the entire range of simulated loads.
3. The dominant frequency of the modeled system as obtained with DDA does not depend on the time interval used (a range of 0.01 to 0.0001 s was analyzed, results for $\Delta t = 0.0001$ s not shown here).
4. Finally, all the dominant frequencies that were obtained with two-dimensional-DDA for the optimal range of penalty values are in the range of the two dominant modes obtained experimentally at the site. This result confirms the validity of two-dimensional-DDA as a site response analysis tool for earthquake engineering.

4. DISCUSSION

A well-known dilemma in dynamic numerical analysis is the best choice of the time step size, because it is not only critical for the stability and efficiency of the solution, but also for its accuracy. In this work, one criterion for selecting an optimal penalty value was the absence of horizontal displacements when subjecting a multiblock column to gravitational load. Inspection of sensitivity analyses results (Table IV) reveals that when using a relatively large time step size of 0.01 s no horizontal displacements are obtained numerically for a larger range of penalty values than when using a relatively small time step of 0.001 s. The absence of horizontal displacements when using the larger time step results from the algorithmic damping effect, as discussed earlier. It should be pointed out, however, that with increased time step size, the numerical error increases and, therefore, a smaller time step would be more desirable, from an accuracy stand point. There is a price to pay; however, when using a smaller time step: stability and gravity turn-on will be achieved after a longer period of real time, because of a lesser algorithmic damping effect. This will require longer CPU time before obtaining a stable solution, an issue that may be a problem when solving a multiblock system, even with fast computers.

The issue of the optimal time step to be used may be studied also in relation to the proposed criteria presented in the section dealing with one-dimensional shear wave propagation. Consider Equation (13) that suggests the following criterion for Δt: $\Delta t < \frac{4}{\omega_{\max}}$. To obtain the lowermost upper bound on the optimal time step size, we can use the highest dominant system frequency as obtained with DDA, 6.3 Hz (Table V), yielding an upper bound of 0.1 s, which agrees with the two values used here in forward analysis. The CFL condition (Equation (14)) when applied here for wave velocity of 3000 m/s and element side length of 0.5 m returns an upper bound value of 0.0002 s that is 1 to 2 orders of magnitude lower than used here for forward analysis.

Numerical accuracy depends on the ratio η, defined eariler (Equation (12)) as the ratio between largest element size and wavelength. The largest element size here is 0.5 m. The wave length may be obtained by Equation (17). For the material, we used the density was $\rho = 2250\,\text{kg/m}^3$, and elastic parameters of $E = 17$ GPa and $\nu = 0.22$, yielding a shear modulus $G = 6.97$ GPa. The period of the incident wave was $T = 0.004$ s, yielding a wavelength $\lambda \sim 7$ m and η of 1/14, which satisfies most of the recommendations discussed earlier. Regarding the penalty value and its effect on numerical results, we have shown that the obtained resonance frequency with DDA is highly dependent upon the choice of k (Table V) with higher dominant frequencies obtained with increasing k values, as illustrated in Figure 23. This is intuitive, because with increasing k value the modeled structure is expected to behave more rigidly. Furthermore, the amplitude of the resonance modes clearly decreases with increasing penalty value, as shown in Figure 23. To obtain an acceptable penalty value for such problems, a preliminary calibration test may be necessary, as performed here (Table IV). Indeed, the best fit penalty value for the field test of 4×10^8 N/m falls well within the acceptable range of penalty values obtained from the preliminary calibration, where a range from 1×10^8 to 1×10^9 N/m proved acceptable.

To choose the optimal k value, we may resort to previously published recommendations and examine them in light of new findings reported here. Shi in his user's manual [24] recommends that

Copyright © 2013 John Wiley & Sons, Ltd.

DOI: 10.1002/eqe

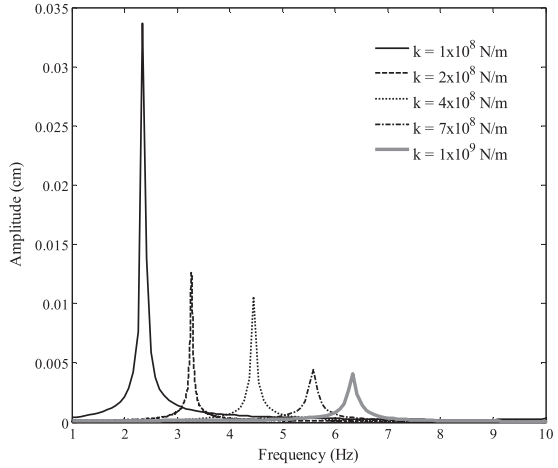

Figure 23. FFT spectra of the displacements of the uppermost block of the column, under five different values of penalty.

$k = (E)(L)$ where E is Young's modulus and L is the average block diameter. In the multidrum column problem modeled here, $E = 17\,\text{GPa}$ and $L = 0.6\,\text{m}$, yielding a recommended k value by Shi of $1 \times 0^{10}\,\text{N/m}^2$, whereas the best fit penalty value found in this study is 1.5 orders of magnitude lower (Table V). Using the recommended k value by Shi would lead to instability of the solution with the Δt selected (Table IV). The reason for the low best fit penalty value with respect to Shi's recommendation could be related to the condition of the interface, its roughness, and the presence of some infilling material between the drums. In the theoretical case of a layered models studied here for comparisons with SHAKE, artificial joints were introduced to optimize the element size, but by doing so, the overall stiffness of the model was reduced because of the springs that are attached at the contacts between elements in DDA. We believe the higher best fit penalty value in those simulations was necessary to offset this numerical artifact. Such a problem does not exist when modeling real field conditions. An interesting note to be made here is that in a previous study [26], we also found that whereas the recommended penalty value by Shi for the monolithic columns studied there was $1.8 \times 10^9\,\text{N/m}$, the best fit between DDA and the analytical solution for the rocking column problem [17] was obtained with a penalty parameter of $8.3 \times 10^7\,\text{N/m}$, also some two orders of magnitude lower than recommended by Shi.

5. SUMMARY AND CONCLUSIONS

The ability of two-dimensional-DDA to perform site response analysis is tested in this paper. We begin with comparisons to SHAKE and proceed with comparisons to geophysical field experiments. To compare between DDA and SHAKE, we use the damping ratio that results in the numerical DDA simulation because of the inherent algorithmic damping, as the assumed damping ratio in SHAKE. We show that by controlling the time step size in DDA, we can actually control the resulting damping ratio, where larger time step results in increased algorithmic damping. The obtained agreement between the two completely different methods is good both in terms of the obtained resonance frequency as well the amplification.

Regarding the optimal relationship between element size (Δx) and wave length (λ), we find that the relative error decreases with decreasing ratio η, where $\eta = \Delta x/\lambda$. We find that this result is independent of time step size. Furthermore, the preservation of the wave shape is also found to be independent of the choice of the time step size. Regarding the optimal penalty value (k) for one-dimensional shear wave propagation when compared with SHAKE, we find that a value of $k = 21 \times EoLo$ (where Eo and Lo are the Young modulus and diameter of the blocks) provides best accuracy. This is a higher penalty parameter than the value of $k = EoLo$ recommended by Shi. We believe the high value of the best fit penalty parameter is necessary in this case to offset the reduction in overall stiffness of the

Copyright © 2013 John Wiley & Sons, Ltd.

DOI: 10.1002/eqe

modeled system due to the introduction of artificial joints. Regarding the influence of the loading mechanism, because we obtain good agreement between DDA, where induced foundation block displacements are used to generate the shear waves, and SHAKE where cyclic accelerations are used in the foundation block, we conclude that the two loading mechanisms are equivalent for site response analysis.

A multidrum column from the World Heritage Site of Avdat is modeled with two-dimensional-DDA, and its dynamic response is compared with experimental data obtained in a geophysical site response survey. Results indicate that DDA returns a resonance frequency range that is very close to the value obtained experimentally. We find that the contact spring stiffness, or penalty value, has a great effect on both the resonance frequency as well as the amplitude as obtained by DDA. The numerically obtained resonance frequency is found to increase with increasing penalty value, whereas its amplitude decreases, as would be expected intuitively. The optimal k value as obtained by comparison between DDA and the physical experiment is found to be $k = (1/25)(EoLo)$, much lower than recommended by Shi. Perhaps, this result reflects the softness of the physical column in reality due to the interfaces between drums, which contain some infilling materials. As in the case of one-dimensional wave propagation, the dominant frequency is found to be independent of the time step size.

ACKNOWLEDGEMENTS

This study is funded by Israel Science Foundation through grant ISF-2201, Contract No. 556/08. Dr. Yuli Zaslavsky and his team from the Geophysical institute of Israel are thanked for conducting the site response analysis survey in Avdat National Park. The people at National Park Authority are thanked for their help and cooperation. Professor Anil K. Chopra and two anonymous reviewers are thanked for their critical comments, which have greatly improved the quality of this paper.

REFERENCES

1. Ambraseys N, Psycharis IN. Earthquake stability of columns and statues. *J Earthquake Eng* 2011; **15**(5): 685–710.
2. Celep Z, Bazant ZP. Spurious reflection of elastic-waves due to gradually changing finite-element size. *Int J Numer Methods Eng* 1983; **19**(5): 631–646.
3. Cheng YM. Advancements and improvement in discontinuous deformation analysis. *Comput Geotech* 1998; **22**(2): 153–163.
4. Chopra AK. *Dynamics of Structures: Theory and Applications to Earthquake Engineering*. Prentice Hall: New Jersey, 2001.
5. Courant R, Friedrichs K, Lewy H. On the partial difference equations of mathematical physics. *IBM J Res Dev* 1967; **11**(2): 215–234.
6. Doolin DM, Sitar N. Time integration in discontinuous deformation analysis. *J. Eng. Mech. ASCE* 2004; **130**(3): 249–258.
7. Fabian P. Evidence of earthquake destruction in the archaeological record - the case of ancient Avedat. *IGS Ann. Meeting*, Mizpe Ramon, 1998.
8. Gu J, Zhao ZY. Considerations of the discontinuous deformation analysis on wave propagation problems. *Int J Numer Anal Methods Geomech* 2009; **33**(12): 1449–1465.
9. Jing L. A review of techniques, advances and outstanding issues in numerical modelling for rock mechanics and rock engineering. *Int J Rock Mech Min Sci* 2003; **40**: 283–353.
10. Kagawa Y, Tsuchiya T, Yamabuchi T, Kawabe H, Fujii T. Finite-element simulation of nonlinear sound-wave propagation. *J Sound Vib* 1992; **154**(1): 125–145.
11. Konstantinidis D, Makris N. Seismic response analysis of multidrum classical columns. *Earthquake Eng Struct Dyn* 2005; **34**(10): 1243–1270.
12. Kramer SL. *Geotechnical Earthquake Engineering*. Prentice-Hall: New Jersey, 1996.
13. Lin CT, Amadei B, Jung J, Dwyer J. Extensions of discontinuous deformation analysis for jointed rock masses. *Int J Rock Mech Min Sci Geomechs Abstr* 1996; **33**(7): 671–694.
14. Lysmer J, Kuhlemeyer RL. Finite dynamic model for infinite media. *J Eng Mech Div, ASCE* 1969; **95**(EM4): 859–877.
15. Lysmer J, Seed HB, Schanable PB. SHAKE - a copmuter program for earthquake response analysis for horizontally layered sites. U. o. C. Rpt. EERC 72–12, Berkeley, 1972.
16. MacLaughlin, MM, Doolin DM. 2006. Review of validation of the discontinuous deformation analysis (DDA) method. *Int J Numer Anal Methods Geomech.* **30**(4): 271–305.
17. Makris N, Roussos YS. Rocking response of rigid blocks under near-source ground motions. *Geotech* 2000; **50**(3): 243–262.
18. Mazor E, Korjenkov A. Applied archeoseismology. *The Makhteshim Country Laboratory of Nature*, Mazor E and Krasnov B (eds). Pensoft: Moscow, 2001; **4**: 123–136.
19. Moser F, Jacobs LJ, Qu JM. Modeling elastic wave propagation in waveguides with the finite element method. *Ndt & E Int* 1999; **32**(4): 225–234.

Copyright © 2013 John Wiley & Sons, Ltd.

DOI: 10.1002/eqe

20. Negev A. The Nabatean cities in the Negev. Ariel, 1988.
21. Ning Y, Zhao Z. A detailed investigation of block dynamic sliding by the discontinuous deformation analysis. *Int J Numer Anal Methods Geomech*, in press.
22. Schnabel PB, Lysmer J, Seed HB. SHAKE: a computer program for earthquake response analysis of horizontally layered sites. Berkeley, Earthquake Engineering Research Center, University of California: 102, 1972.
23. Shi G. *Block System Modeling by Discontinuous Deformation Analysis*. Computational Mechanics Publication: Southhampton, UK, 1993.
24. Shi G. Discontinuous deformation analysis programs, version 96, user's manual. R. M.-C. Young, 1996.
25. Wu JH. Seismic landslide simulations in discontinuous deformation analysis. *Comput Geotech* 2010; **37**(5): 594–601.
26. Yagoda-Biran G, Hatzor YH. 2010. Constraining paleo PGA values by numerical analysis of overturned columns. *Earthquake Eng Struc* **39**(4): 463–472.
27. Zaslavsky Y, Perelman N, Kalmanovich M, Shvartsburg A, Portnov P. Experimental assessment of dynamic characteristics of two momuments in Avdat National Park. 562/608/11, Geophysical Institute of Israel, 2011.

Copyright © 2013 John Wiley & Sons, Ltd.

DOI: 10.1002/eqe